In situ transmission electron microscopy investigation of the interfacial reaction between Ni and Al during rapid heating in a nanocalorimeter

Michael D. Grapes, Thomas LaGrange, Karsten Woll, Bryan W. Reed, Geoffrey H. Campbell, David A. LaVan, and Timothy P. Weihs

Citation: APL Materials **2**, 116102 (2014); doi: 10.1063/1.4900818

View online: https://doi.org/10.1063/1.4900818

View Table of Contents: http://aip.scitation.org/toc/apm/2/11

Published by the American Institute of Physics

In situ transmission electron microscopy investigation of the interfacial reaction between Ni and Al during rapid heating in a nanocalorimeter

Michael D. Grapes,[1,2,a] Thomas LaGrange,[3] Karsten Woll,[1,4] Bryan W. Reed,[3] Geoffrey H. Campbell,[3] David A. LaVan,[2,a] and Timothy P. Weihs[1,a]

[1]*Department of Materials Science and Engineering, Johns Hopkins University, Baltimore, Maryland 21218, USA*
[2]*Material Measurement Laboratory, Materials Measurement Science Division, National Institute of Standards and Technology, Gaithersburg, Maryland 20899, USA*
[3]*Lawrence Livermore National Laboratory, Materials Science and Technology Division, Livermore, California 94550, USA*
[4]*Institute of Applied Materials, Karlsruhe Institute of Technology, 76344 Eggenstein-Leopoldshafen, Germany*

(Received 6 May 2014; accepted 20 October 2014; published online 3 November 2014)

The Al/Ni formation reaction is highly exothermic and of both scientific and technological significance. In this report, we study the evolution of intermetallic phases in this reaction at a heating rate of 830 K/s. 100-nm-thick Al/Ni bilayers were deposited onto nanocalorimeter sensors that enable the measurement of temperature and heat flow during rapid heating. Time-resolved transmission electron diffraction patterns captured simultaneously with thermal measurements allow us to identify the intermetallic phases present and reconstruct the phase transformation sequence as a function of time and temperature. The results show a mostly unaltered phase transformation sequence compared to lower heating rates. [http://dx.doi.org/10.1063/1.4900818]

Thin film and interfacial reactions have been studied extensively for many years. These reactions are of broad interest both in industry (e.g., for microelectronics,[1,2] microelectromechanical systems,[3,4] and coatings[5]) and in science, where reduced diffusion distances and increased surface area provide an opportunity to study phase formation in a unique environment.[6–9] One of the best characterized thin film reactions is between Al and Ni.[10–20] Al and Ni have a large, negative heat of mixing, making the reaction highly exothermic. Multilayer foils consisting of nanoscale layers of Al and Ni can release this energy very quickly. When a multilayer foil is ignited at one end in a free-standing configuration, the heat released locally is sufficient to ignite the adjacent material and produce a high-velocity reaction front in what is known as a "self-propagating" reaction.[11] Heating rates when reacting in this mode exceed 10^6 K/s. Because of their ability to deliver rapid, local heating, Al/Ni multilayer foils have been exploited as heat sources for rapid room-temperature soldering.[12,13]

In order to better understand the reaction in Al/Ni multilayers, many studies have identified the sequence of phases that form as the multilayers are heated.[14–17] Historically, these studies have been accomplished using differential scanning calorimetry. These instruments heat a sample at a controlled rate that is typically less than 1 K/s and measure the heat evolved as a function of temperature. The phase(s) present at different points during the heating cycle are determined by quenching and analyzing the sample with x-ray diffraction. More recently, there has been interest in studying the phase transformations during self-propagation of these reactions, where heating rates are approximately one-million times higher. Since quenching is difficult for reactions progressing at these rates, *in situ*

[a]mgrapes1@jhu.edu; david.lavan@nist.gov; and weihs@jhu.edu

characterization methods are preferred in this regime. To-date such studies have been accomplished using two techniques: synchrotron x-ray microdiffraction[18,19] and time-resolved transmission electron microscopy (TEM).[20]

For multilayers with a 1:1 Al:Ni atomic ratio, slow heating experiments typically have identified two phase transformation sequences depending on the deposition method. For evaporated Al/Ni multilayers,[14,21] the phase transformation sequence under slow heating is

$$\mathrm{Al + Ni \rightarrow Al_3Ni + Ni \rightarrow Al_3Ni_2 + Ni \rightarrow AlNi.} \quad (1)$$

For Al/Ni multilayers that are deposited by sputtering or ion-beam deposition, the sequence is altered slightly[15,17]

$$\mathrm{Al + Ni \rightarrow Al_9Ni_2 + Ni \rightarrow Al_3Ni + Ni \rightarrow Al_3Ni_2 + Ni \rightarrow AlNi.} \quad (2)$$

The distinction between these two sequences is in the first phase to form and is attributed to subtle differences in the initial microstructure of the as-deposited Al/Ni interfaces. These interfaces tend to be more intermixed in sputtered and ion-beam deposited samples, which in turn can impact the nucleation of the Al_9Ni_2 and Al_3Ni phases which have similar free energies of formation.[17]

When sputter-deposited Al/Ni multilayers are reacted in the rapid, self-propagating mode (heating rates exceeding 10^6 K/s) and characterized using synchrotron x-ray diffraction[18,19] or time-resolved TEM,[20] the observed phase transformation sequence becomes

$$\mathrm{Al + Ni \rightarrow Al\text{-}rich\ liquid + Ni \rightarrow AlNi.} \quad (3)$$

Note that while at low heating rates we observe a sequence of solid intermetallic phases, at high heating rates all of the intermetallic phases are skipped and instead mixing occurs in a molten Al-rich phase. The shift in phase sequence with heating rate is attributed to a reduction in the amount of atomic intermixing that occurs prior to reaching temperatures where the intermediate intermetallic phases are no longer stable.[18] To-date this characterization has only been performed on sputtered Al/Ni multilayers, but evaporated multilayers are likely to exhibit the same sequence given that the vast majority of mixing occurs through Ni dissolving into molten Al.

To study this phenomenon over a broad range of heating rates, this work seeks to demonstrate that one can characterize the AlNi formation reaction at heating rates in the 10^3 K/s–10^5 K/s range, intermediate between the heating rates in differential scanning calorimetry (DSC) studies and in self-propagating reactions. Given that these heating rates are orders of magnitude larger than what is possible using a standard DSC, we employ a calorimetric technique that is capable of more rapid heating: nanocalorimetry. A nanocalorimeter is a microelectromechanical device whose miniscule heat capacity enables it to achieve very high heating rates.[22] However, as in self-propagating reactions, analyzing the phases formed at these heating rates is difficult using quenching and *ex situ* observations. Thus, an *in situ* approach is preferred so that phases can be detected as they appear. In this work, we utilize a newly developed *in situ* nanocalorimetry system[23] that makes use of the dynamic transmission electron microscope[24] (DTEM) to perform structural characterization during the calorimetry experiment. The DTEM is a time-resolved TEM designed, built, and housed at Lawrence Livermore National Laboratory.

The *in situ* nanocalorimetry system is depicted schematically in Fig. 1 and consists of the DTEM itself, TEM-compatible nanocalorimeter sensors, an *in situ* nanocalorimetry TEM holder, and a data acquisition system. The DTEM utilizes an ultraviolet-laser-driven photocathode to produce extremely short, high-intensity electron pulses.[24] The laser intensity and duration can be manipulated to create electron pulses from 30 ns to 500 ns in length. Nanocalorimeters consist of a platinum strip for heating and temperature measurement suspended on a silicon nitride membrane to minimize heat losses and thermal mass.[22] The temperature-resistance relationship for each sensor is calibrated optically[25] prior to first use, and for TEM investigation, the sensor design was modified to include three 100 μm × 100 μm electron-transparent windows in the platinum strip.[23] After a sample is deposited on the sensor it is placed into a custom-built *in situ* nanocalorimetry holder which is compatible with the DTEM goniometer. This holder provides electrical connections between the Pt sensor and a data acquisition system that is synchronized with the DTEM via a custom-built LabVIEW interface.

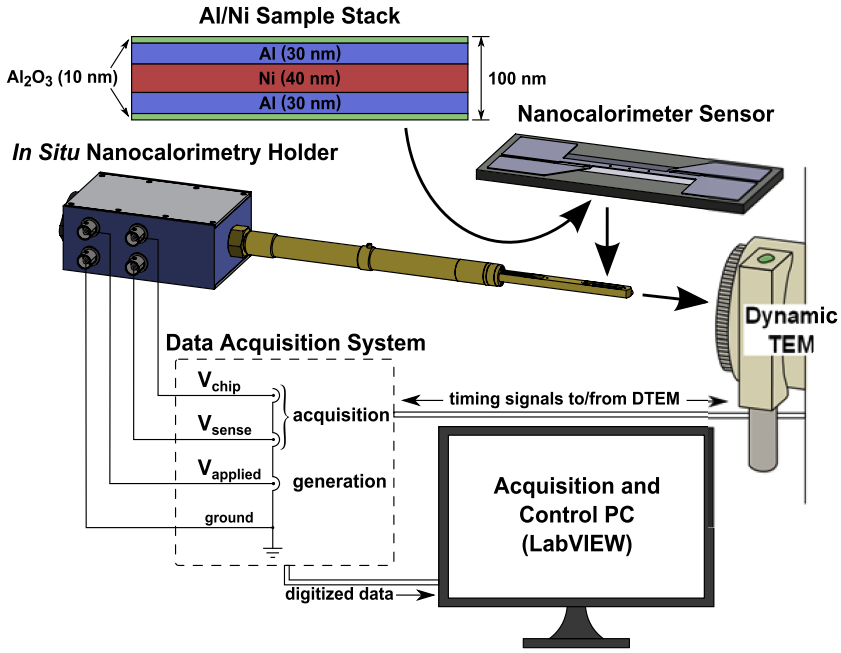

FIG. 1. Schematic of the experimental system for *in situ* nanocalorimetry showing a nanocalorimeter sensor, the *in situ* nanocalorimetry holder, the dynamic TEM, and the data acquisition system. Also shown is the sample geometry studied in this work, a 100 nm thick Ni/Al bilayer.

Full details on the design and operation of the *in situ* nanocalorimetry system have been reported elsewhere.[23]

The samples tested in this study consisted of 40 nm of Ni (target purity 99.995%) sandwiched between two 30 nm layers of Al (target purity 99.999%) for a total bilayer thickness of 100 nm and an overall composition of 50 at. % of Al. This sandwich structure is the smallest symmetric repeat unit of a multilayer with a 100 nm bilayer spacing and matches the structure used in previous nanocalorimetry investigations of the Al/Ni reaction.[26] 10 nm of Al_2O_3 was deposited on both sides of the Al/Ni/Al stack to serve as a passivation layer and diffusion barrier. This sample geometry is illustrated in the upper-left of Fig. 1. The sample stack was deposited through a shadow-mask directly onto the underside of the nanocalorimeter sensor by e-beam evaporation. Layer thickness during deposition was measured by a quartz crystal thickness monitor. For the experiments reported here, the DTEM was configured for single-shot mode with an electron-pulse-duration of 500 ns. Selected-area electron diffraction patterns were collected with a $\approx$0.55 μm^2 selected-area aperture positioned in the central electron window of the nanocalorimeter heater strip. Since the Al/Ni formation reaction is irreversible, four nanocalorimeters containing identical samples were reacted and imaged at different times to construct a full picture of the phase formation sequence. The average heating rate during the experiments was 830 K/s.

Characteristic results from the nanocalorimetry system during the heating segment of one experiment are presented in Fig. 2. The plot of temperature vs. time in Fig. 2(a) depicts the measurable difference in the temperature evolution of the sample during the first heating (when a reaction is occurring) as compared to the second heating (when the reactants have already been consumed). This difference can be extracted and quantified to give the reaction power, the rate of heat release that is due to a reaction in the sample and not external heating, shown in Fig. 2(b). Note the presence of two large exothermic peaks with one small exothermic peak in between them. These peaks are highlighted by fitting each with a Voigt distribution in Fig. 2(b). An alternative way to display nanocalorimetry results is to plot dH/dT vs. temperature, shown in Fig. 2(c). This curve is the temperature-domain equivalent of Fig. 2(b) and can be helpful in understanding how reaction rates change with temperature. The quantity dH/dT is computed by dividing the total reaction power by the heating rate, and the fit peaks

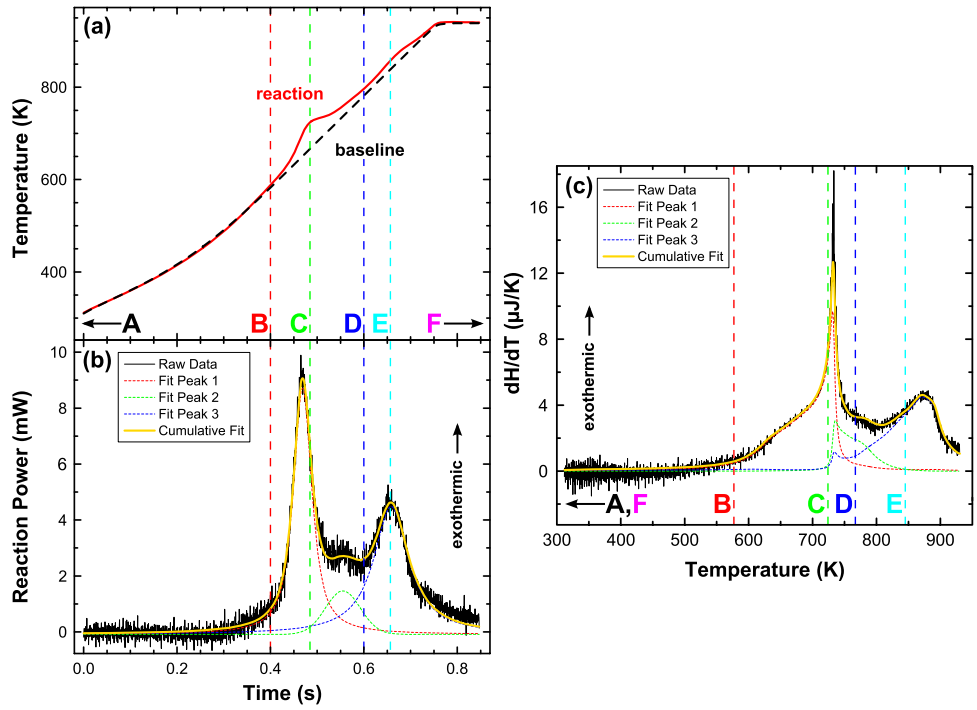

FIG. 2. Typical nanocalorimetry data for a 100 nm Al/Ni bilayer heated at an average rate of 830 K/s: (a) temperature vs. time for two consecutive scans showing the temperature excursion when a reaction occurs, (b) reaction power vs. time showing heat evolution in three distinct exothermic peaks fitted with Voigt distributions, and (c) dH/dT vs. temperature showing the shape of the three exothermic peaks in the temperature domain. The dashed lines indicate the points at which the diffraction patterns in Fig. 3 were taken. The FWHM for the three fitted peaks in (b) is 33 ms, 95 ms, and 86 ms, respectively.

and cumulative fit shown in Fig. 2(c) were calculated by dividing the peak fits in Fig. 2(b) by the heating rate as well.

Electron diffraction patterns were captured using the DTEM at the times indicated in Fig. 2 in order to identify the phase transformations occurring in each of the three exotherms. In addition to the four electron diffraction patterns captured during the heating experiment (B–E), patterns were also taken at room temperature before (A) and after (F) to identify the initial and final phases. Fig. 3 presents these results as a sequence of 1D diffraction patterns, obtained by rotational averaging of the original 2D patterns followed by background subtraction. All observable peaks are labeled with the most likely phase or phases. We also label the temperature of the sample when the pattern was captured and the amount of heat that had been released up to that point (as a percentage of the total theoretical heat of formation for AlNi). The sequence is described below.

Pattern A presents the initial state of the sample prior to heating. All of the measured diffraction peaks can be attributed to either fcc Al or fcc Ni. Pattern B is the first pattern captured during the heating experiment. It represents a 280 K temperature increase over pattern A but still represents a pre-reaction microstructure (3% reaction completion). As such, it shows essentially no changes from pattern A other than slight peak broadening and a slight shift to smaller $1/d$ due to thermal expansion. Pattern C was captured more than half-way through the first exotherm as shown in Fig. 2(b). Here we see the first clear evidence of a reaction, as the fcc Al peaks have disappeared and have been replaced by peaks from Al_3Ni ($oP16$ structure[27]). Al_3Ni has an exceptionally large number of diffraction peaks (over 450 in the range shown) that are too weak to detect individually in these experiments. However, in certain regions, these peaks overlap to give measurable intensities distinct from those of fcc Ni. These regions are labeled in Fig. 3 and include a broad peak around 2.72 nm^{-1} (formed by the (011), (101), (020), (111), and (200) reflections) and a shoulder around 4.07 nm^{-1} (formed by the (211), (220), and (002) reflections). Note that in this pattern, and in the two that follow, the prominent peak around 4.9 nm^{-1} cannot be used for phase identification because all of the candidate phases have

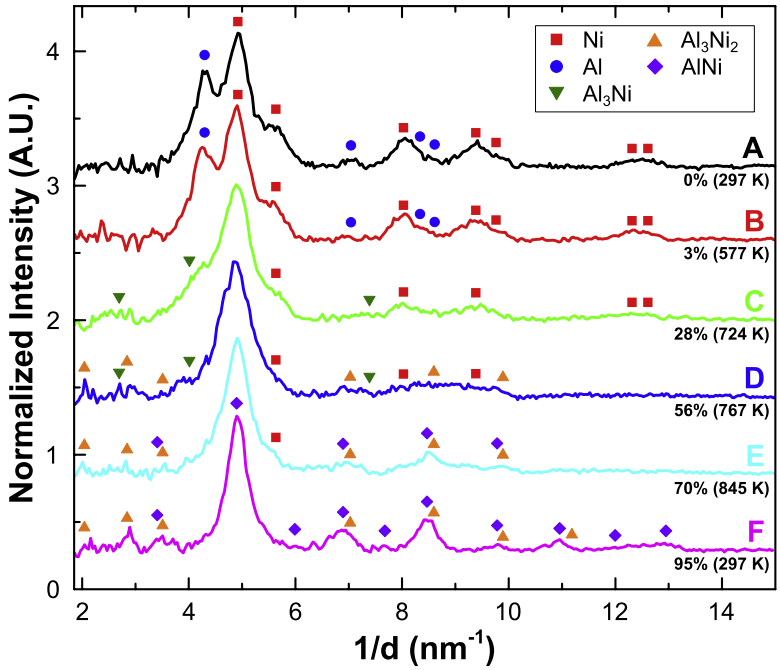

FIG. 3. Time-resolved electron diffraction patterns captured before, during, and after the reaction of a 100 nm Al/Ni bilayer. The pattern labels correspond to the times in Fig. 2. Also labeled for each pattern is the percentage of heat released (as a fraction of the theoretical enthalpy of formation) and the temperature when the pattern was captured. The prominent peak around 4.9 nm^{-1} is unlabeled for patterns C–E because all of the intermetallic phases have one or more peaks in this region, and the peak is too broad to distinguish between them.

large peaks in this region. Pattern D represents the state of the sample near the end of the second, small exotherm. Diffraction peaks from Ni and Al_3Ni are still visible but this pattern shows the first clear evidence for the Al_3Ni_2 phase (*hP*5 structure[27]) in the form of the (001) peak at 2.04 nm^{-1} and the (202)/(022) peak at 7.03 nm^{-1}. There is some evidence for the (100) peak at 2.86 nm^{-1} and the (212)/(122) peak at 8.60 nm^{-1} but the former is obscured by the nearby Al_3Ni peaks while the latter combines with the shrinking (220) and (311) Ni peaks to form a relatively featureless signal around 8.9 nm^{-1}. In pattern E, acquired in the middle of the final exotherm, the signal from fcc Ni has almost disappeared except for the shoulder at 5.64 nm^{-1} due to the (200) peak. This makes it easier to see clear peaks due to the Al_3Ni_2 phase. Peaks from AlNi (*cP*2 structure[27]) may also be contributing, but it is very difficult to distinguish between AlNi and Al_3Ni_2 when the peaks are broad unless the AlNi (111) and (210) superlattice peaks at 6.00 nm^{-1} and 7.75 nm^{-1} are visible. This difficulty persists in pattern F, which shows the final room temperature state of the sample after the heating experiment. There is some evidence for the AlNi superlattice peaks but the persistence of Al_3Ni_2 peaks at 2.04 nm^{-1} and 2.86 nm^{-1} suggests that the primary phase is still Al_3Ni_2.

The reaction power in Fig. 2(b) shows three distinct exotherms. Fitting the exothermic peaks and taking the integral of the cumulative fit curve yields the total heat evolved. Averaged over the four samples reported the total heat is 1.25 mJ with a standard deviation of 0.042 mJ. The sample mass can be estimated using the intended layer thicknesses, the estimated sample area (3.7 mm × 0.5 mm), and the bulk densities for Al and Ni. We estimate the mass in this way to be 960 ng yielding a normalized average heat of formation of 1302 J g^{-1} ± 44 J g^{-1}. This is 5.7% ∓ 3.2% lower than the theoretical value for AlNi,[28] 1381 J g^{-1}. Since Al_3Ni_2 peaks are still visible in the final diffraction pattern, an incomplete reaction is likely responsible for at least part of this discrepancy. Uncertainty in the estimation of the sample mass may also be a contributing factor. Comparing the positions of the exothermic peaks in Fig. 2 to the electron diffraction patterns in Fig. 3, we conclude that the first exotherm in the nanocalorimetry data corresponds to the formation of Al_3Ni, the second to an initial stage of Al_3Ni_2 formation, and the third to a second stage of Al_3Ni_2 growth and transformation to AlNi. Thus, the overall phase sequence observed in these experiments is the same as that presented in Eq. (1) for

evaporated Al/Ni layers under slow heating. However, it appears that in these experiments Al_3Ni_2 grows in a two-stage mode, something that has not been reported previously for this phase.

Two facts support the conclusion that Al_3Ni_2 formation occurs across both the second and third exotherms: (1) rather than disappearing, the Al_3Ni_2 diffraction peaks grow stronger between patterns D and E which span the third exotherm, and (2) the area of the second exothermic peak is too small for complete formation of Al_3Ni_2 to have occurred. Specifically, in these experiments the second exotherm contributes 10% of the theoretical heat of formation, while literature values for Al_3Ni_2 indicate that the formation of this phase should account for about 38% of the total heat.[29] Based on this argument, Al_3Ni_2 must continue to grow during the third exotherm. The best explanation for a phase forming in multiple exotherms comes from the model proposed by Coffey *et al.*, where the first exothermic peak corresponds to the formation of an interfacial layer of the new phase and the second exothermic peak indicates 1D growth of this layer through the remaining reactants.[30] For a 100 nm bilayer, we expect that the second exotherm should be substantially larger than the first exotherm, so this model is a good fit for the data we have obtained. The shape of the third peak in Fig. 2(c) is also consistent with this explanation as it displays the gradual rise and rapid fall-off characteristic of diffusion-limited growth.[31]

Going forward, one line of investigation will be to extend the present work on the 1:1 Al:Ni composition to higher heating rates where more significant changes in phase formation sequence may occur. However, since characteristic reaction temperatures increase as the heating rate increases,[32] there may be a limit on the maximum heating rate that can be studied while still forming the final AlNi phase. In light of this, a second line of investigation will be to study films with the Al-rich compositions of 3:1 and 3:2 Al:Ni (corresponding to the Al_3Ni and Al_3Ni_2 intermetallic phases). By excluding the formation of the highest temperature phase, AlNi, these samples will allow us to study the formation of the Al_3Ni and Al_3Ni_2 intermetallics at heating rates up to the maximum rates possible using nanocalorimetry.

More generally, the *in situ* nanocalorimetry system demonstrated here can be applied to study rapid phase transformations and microstructural changes in a number of fields, for example, in the study of bulk metallic glasses. Traditional calorimeters operate at heating and cooling rates that are too low to induce amorphization in these materials but nanocalorimetry has been shown to be capable of achieving these rates and measuring the enthalpy of the transformation directly.[33,34] This *in situ* nanocalorimetry system would extend that capability by offering the time resolution required to actually observe the amorphization process as it occurs. For studies requiring even more extreme heating and cooling rates, the *in situ* nanocalorimeter could be operated as a dedicated calorimetric sensor in combination with a laser for localized heating. This would extend the potential applications to include simultaneous structural and calorimetric measurements of amorphous melting in Si and Ge[35,36] and of the amorphization and crystallization processes in phase change materials.[37]

In conclusion, we have demonstrated that one can study rapid phase transformations in 1:1 Al:Ni bilayers using a new system combining *in situ* nanocalorimetry and DTEM. The intermediate phases in the reaction were identified using *in situ* electron diffraction for samples heated at an average heating rate of 830 K/s. Nanocalorimeter data indicate that at this heating rate, the formation reaction occurs in a sequence of three exotherms producing approximately 95% of the theoretical heat of formation for this stoichiometry. Meanwhile, *in situ* time-resolved electron diffraction confirms that the phase transformation sequence is similar to that observed at much slower heating rates in a DSC, $Al + Ni \rightarrow Al_3Ni + Ni \rightarrow Al_3Ni_2 + Ni \rightarrow AlNi$. The 5% discrepancy in total heat of formation likely appears because the final reaction step did not go to completion, an explanation supported by the persistence of Al_3Ni_2 diffraction peaks in the electron diffraction patterns of as-reacted samples. Future work on the Al/Ni system will aim to analyze the phase transformation sequence for 1:1 Al:Ni bilayers at higher heating rates and to study bilayers with 3:1 and 3:2 Al:Ni compositions in order to gain a better understanding of the processes by which the Al_3Ni and Al_3Ni_2 intermetallic phases form.

The authors are grateful to Bernadette Cannon for her help calibrating nanocalorimeter sensors during her time as a Summer Undergraduate Research Fellowship student at the National Institute of Standards and Technology (NIST). M.D.G. and T.P.W. were supported in part by NIST

Grant No. 70NANB9H9146 and in part by National Science Foundation Grant No. DMR-1308966. M.D.G., K.W., and T.P.W. were supported in part by U.S. Department of Energy Grant No. DE-FG02-09ER46648. Nanocalorimeter fabrication was performed at the NIST Center for Nanoscale Science & Technology. The work presented in this article was conducted at the Lawrence Livermore National Laboratory (LLNL) DTEM facility under the auspices of the U.S. Department of Energy by LLNL under Contract No. DE-AC52-07NA27344. The DTEM experiments conducted at LLNL and effort of T.L., B.W.R., and G.H.C. were supported by the U.S. Department of Energy, Office of Basic Energy Sciences, Division of Materials Science and Engineering under FWP SCW0974. Certain commercial equipment, instruments, or materials are identified in this document. Such identification does not imply recommendation or endorsement by the National Institute of Standards and Technology, nor does it imply that the products identified are necessarily the best available for the purpose. Since the completion of this work, T.L. and B.W.R. have become employees at Integrated Dynamic Electron Solutions, Inc., a start-up company marketing time-resolved electron microscope technology. Publication of this article was funded in part by the Open Access Promotion Fund of the Johns Hopkins University Libraries.

[1] F. M. d'Heurle, J. Mater. Res. **3**, 167 (1988).
[2] R. Rosenberg, D. C. Edelstein, C.-K. Hu, and K. P. Rodbell, Annu. Rev. Mater. Sci. **30**, 229 (2000).
[3] Y. Fu, H. Du, W. Huang, S. Zhang, and M. Hu, Sens. Actuators, A **112**, 395 (2004).
[4] Y. Shacham-Diamand and Y. Sverdlov, Microelectron. Eng. **50**, 525 (2000).
[5] M. J. Pomeroy, Mater. Des. **26**, 223 (2005).
[6] K. F. Kelton and A. L. Greer, *Nucleation in Condensed Matter: Applications in Materials and Biology* (Elsevier, 2010).
[7] U. Gösele and K. N. Tu, J. Appl. Phys. **53**, 3252 (1982).
[8] F. Hodaj and A. M. Gusak, Acta Mater. **52**, 4305 (2004).
[9] R. J. Highmore, Philos. Mag. B **62**, 455 (1990).
[10] E. G. Colgan, Mater. Sci. Rep. **5**, 1 (1990).
[11] E. Ma, C. V. Thompson, L. A. Clevenger, and K. N. Tu, Appl. Phys. Lett. **57**, 1262 (1990).
[12] J. Wang, E. Besnoin, A. Duckham, S. J. Spey, M. E. Reiss, O. M. Knio, M. Powers, M. Whitener, and T. P. Weihs, Appl. Phys. Lett. **83**, 3987 (2003).
[13] X. Qiu and J. Wang, Sens. Actuators, A **141**, 476 (2008).
[14] E. Ma, C. V. Thompson, and L. A. Clevenger, J. Appl. Phys. **69**, 2211 (1991).
[15] A. S. Edelstein, R. K. Everett, G. Y. Richardson, S. B. Qadri, E. I. Altman, J. C. Foley, and J. H. Perepezko, J. Appl. Phys. **76**, 7850 (1994).
[16] C. Michaelsen, G. Lucadamo, and K. Barmak, J. Appl. Phys. **80**, 6689 (1996).
[17] K. J. Blobaum, D. Van Heerden, A. J. Gavens, and T. P. Weihs, Acta Mater. **51**, 3871 (2003).
[18] J. C. Trenkle, L. J. Koerner, M. W. Tate, N. Walker, S. M. Gruner, T. P. Weihs, and T. C. Hufnagel, J. Appl. Phys. **107**, 113511 (2010).
[19] K. Fadenberger, I. E. Gunduz, C. Tsotsos, M. Kokonou, S. Gravani, S. Brandstetter, A. Bergamaschi, B. Schmitt, P. H. Mayrhofer, C. C. Doumanidis, and C. Rebholz, Appl. Phys. Lett. **97**, 144101 (2010).
[20] J. S. Kim, T. LaGrange, B. W. Reed, R. Knepper, T. P. Weihs, N. D. Browning, and G. H. Campbell, Acta Mater. **59**, 3571 (2011).
[21] T. S. Dyer and Z. A. Munir, Metall. Mater. Trans. B **26**, 603 (1995).
[22] E. A. Olson, M. Y. Efremov, and L. H. Allen, J. Microelectromech. Syst. **12**, 355 (2003).
[23] M. D. Grapes, T. LaGrange, L. H. Friedman, B. W. Reed, G. H. Campbell, T. P. Weihs, and D. A. LaVan, Rev. Sci. Instrum. **85**, 084902 (2014).
[24] B. W. Reed, T. LaGrange, R. M. Shuttlesworth, D. J. Gibson, G. H. Campbell, and N. D. Browning, Rev. Sci. Instrum. **81**, 053706 (2010).
[25] P. Swaminathan, B. G. Burke, A. E. Holness, B. Wilthan, L. Hanssen, T. P. Weihs, and D. A. LaVan, Thermochim. Acta **522**, 60 (2011).
[26] P. Swaminathan, M. D. Grapes, K. Woll, S. C. Barron, D. A. LaVan, and T. P. Weihs, J. Appl. Phys. **113**, 143509 (2013).
[27] P. Villars and L. D. Calvert, *Pearson's Handbook of Crystallographic Data for Intermetallic Phases*, 2nd ed. (ASM international, 1991).
[28] S. H. Fischer and M. C. Grubelich, *in 32nd Joint Propulsion Conference and Exhibit* (American Institute of Aeronautics and Astronautics, Reston, Virigina, 1996).
[29] F. R. de Boer, R. Boom, W. C. M. Mattens, A. R. Miedema, and A. K. Niessen, *Cohesion in Metals* (North-Holland Physics Publishing, 1988), p. 309.
[30] K. R. Coffey, L. A. Clevenger, K. Barmak, D. A. Rudman, and C. V. Thompson, Appl. Phys. Lett. **55**, 852 (1989).
[31] C. Michaelsen, K. Barmak, and T. P. Weihs, J. Phys. D: Appl. Phys. **30**, 3167 (1997).
[32] H. E. Kissinger, Anal. Chem. **29**, 1702 (1957).
[33] J. M. Gregoire, P. J. McCluskey, D. Dale, S. Ding, J. Schroers, and J. J. Vlassak, Scr. Mater. **66**, 178 (2012).
[34] P. J. McCluskey and J. J. Vlassak, Scr. Mater. **64**, 264 (2011).
[35] M. Thompson, G. Galvin, J. Mayer, P. Peercy, J. Poate, D. Jacobson, A. Cullis, and N. Chew, Phys. Rev. Lett. **52**, 2360 (1984).
[36] P. Baeri, G. Foti, J. Poate, and A. Cullis, Phys. Rev. Lett. **45**, 2036 (1980).
[37] M. Wuttig and N. Yamada, Nat. Mater. **6**, 824 (2007).